# Undulator-Induced Transparency of Magnetized Plasma: New Approach to Electromagnetic Energy Compression

Mikhail Tushentsov, Gennady Shvets, *Member, IEEE*, Andrey Yu. Kryachko, and Mikhail D. Tokman

***Abstract*—It is well known that circularly polarized electromagnetic waves propagating along the magnetic field in the plasma are strongly absorbed when the wave frequency matches the electron cyclotron frequency. This absorption can be eliminated by adding a weak magnetic undulator, leading to the undulator-induced transparency (UIT) of the plasma. Moreover, the group velocity of the waves in the plasma is strongly reduced, resulting in the extreme compression of the wave energy in the plasma. Compressed waves are polarized along the propagation direction and can be used for synchronous electron or ion acceleration. Numerical simulations reveal yet another interesting property of the electromagnetic waves in UIT plasma: strong coupling and conversion between two circular wave polarizations. Depending on how important this cross-polarization effect is, several propagation regimes have been identified and explored by fluid and particle-in-cell simulations.**

***Index Terms*—Energy compression, microwave-plasma interactions, plasma accelerators.**

## I. Introduction and Overview of Earlier Work

IMAGINE a material with a refractive index equal to unity through which a narrow-band electromagnetic wave with frequency $\omega$ and wavenumber $k = \omega/c$ can propagate with the group velocity $v_g = \partial\omega/\partial k \ll c$, where $c$ is the speed of light in vacuum. Such a material could serve as a perfect compressor of the electromagnetic energy: an electromagnetic wave incident on a material slab would not undergo any reflections due to the perfect impedance matching with vacuum, yet be compressed in length by a factor $G = c/v_g \gg 1$. Although such materials do not exist in nature, they have been synthesized in the laboratory. The phenomenon enabling such materials is the electromagnetically induced transparency (EIT) [1], [2]. EIT enables propagation of an electromagnetic wave through the normally opaque medium in the presence of a second, more powerful electromagnetic wave. Although EIT was first predicted and observed in gases, it was later extended to solids [3], [4]. Regardless of the medium in which EIT is implemented, its most desirable manifestation is the dramatic slowing down (or even stopping) of electromagnetic waves. For example, it has been suggested that strong coupling between electromagnetic and acoustic waves can be realized by slowing down light to the sound speed [5].

It has recently been shown that EIT is possible not only in quantum mechanical systems (as it was initially believed), but also in classical systems such as the magnetized plasma [6]–[8]. A right-hand circularly polarized (RHCP) electromagnetic wave launched along the magnetic field $\boldsymbol{B} = B_0\boldsymbol{e}_z$ and having the frequency $\omega_1 = \Omega_0$ (where $\Omega_0 = eB_0/mc$ is the electron cyclotron frequency) is resonantly absorbed by the plasma: the phenomenon is known as electron cyclotron heating (ECH). The left-hand circularly polarized (LHCP) wave propagates without absorption. Transparency of the plasma to RHCP wave is achieved, and ECH overcome by adding a lower-frequency pump with $\omega_0 = \Omega_0 - \omega_p$, where $\omega_p = (4\pi e^2 N/m)^{1/2}$ is the electron plasma frequency. Here, $N$ is the plasma density, $-e$ is the electron charge, and $m$ is the electron mass. In the special case of $\Omega_0 = \omega_p$, the frequency of the pump is equal to zero, corresponding to a magnetostatic undulator with $\boldsymbol{B}_u = B_u(\boldsymbol{e}_x \cos k_u z - \boldsymbol{e}_y \sin k_u z)$ as a pump. A simple energy level schematic demonstrating the analogy between the classical and quantum mechanical regimes of EIT is shown in [9].

Undulator induced transparency [9] (UIT) is the easiest to realize experimentally because it does not rely on high-power pump radiation. All that is needed is a strong helical undulator with the field strength $B_u$. Cyclotron absorption is suppressed because of the excitation of the longitudinal plasma wave (plasmon). Magnetostatic undulator couples the longitudinal plasma and the transverse RHCP waves resulting in a hybrid wave which has both longitudinal and transverse components of the electric field. The hybrid wave is not absorbed at the cyclotron frequency, which is the signature of the UIT of plasma. Because of the practically achievable axial and undulator magnetic field strengths $B_0$ and $B_u$, UIT is a microwave/plasma phenomenon with an upper frequency bound of about 300 GHz.

The group velocity of the hybrid wave can be very slow for $B_u \ll B_0$, making the hybrid wave the equivalent of the slow light in quantum optics. The slowing down occurs because the hybrid wave is primarily longitudinally polarized and has a small Poynting vector. If the spatial length of the injected electromagnetic wave is $L_0 = c\tau_0$ (where $\tau_0$ is the temporal pulse duration), the spatial length of the hybrid wave is $L_1 = v_g\tau_0 \ll L_0$, resulting in the energy density increase by a factor $L_0/L_1 = G \gg 1$. The hybrid nature of the slow wave in the plasma bears a strong similarity to the coupled excitations of the light and matter: the so-called dark-state

Manuscript received July 26, 2004; revised October 27, 2004. This work was supported in part by the U.S. Department of Energy under Contracts DE-FG02-04ER54763 and DE-FG02-04ER41321 and in part by the Russian Foundation for Basic Research under Grant 03-02-17 234.

M. Tushentsov and G. Shvets are with the Physics Department and Institute for Fusion Studies, The University of Texas, Austin, TX 78712 USA.

A. Yu. Kryachko and M. D. Tokman are with the Institute of Applied Physics, Russian Academy of Sciences, 603600 Nizhny Novgorod, Russia.

Digital Object Identifier 10.1109/TPS.2004.841927

polaritons [10]. The essential difference is that the slowing down of light due to creation of dark-state polaritons does not amount to energy compression: most of the compressed pulse energy is carried away by the pump, plus some is stored in the atoms. In UIT, the pump is magnetostatic and cannot carry away energy. Therefore, the entire pulse energy is compressed.

One of the promising applications of the compressed energy in the plasma is the high-gradient acceleration of electrons and ions which is made even more attractive by the ability to tune the phase velocity of the accelerating field [11]. Other applications include pulse chopping and selective plasma heating. For all these applications it is desirable to have as large compression as possible. The earlier linearized analytic models (fluid [6], Lagrangian [7], and kinetic [8]) assumed that the hybrid wave has a single helicity (e.g., RHCP, wave propagating in the positive $z$-direction). The analytic predictions of the single-helicity theory is that the group velocity of the hybrid wave (RHCP plus the electron plasma wave) is given by $v_g = (B_u/B_0)^2 c/2$ [7]. Therefore, it is advantageous to achieve UIT with as small $B_u$ as plasma homogeneity allows. Earlier particle-in-cell (PIC) simulations [11] have confirmed UIT for $B_u \geq 0.5B_0$ but failed to find transparency for smaller values of $B_u$. Moreover, a peculiar and unaccounted for by the analytic model dependence of the wave propagation on the undulator period and helicity has been revealed [11] by the PIC simulations.

Here we investigate a new physical effect, coupling between the RHCP and LHCP waves, which accounts for these dependencies. It is found that the assumption of the single helicity of the hybrid wave is violated due to this coupling, and the predictions of the single-helicity theory must be modified. Using analytic arguments and a linearized fluid code, the ranges of undulator periods and strengths for which the single-helicity theory is valid and pulse compression occurs are found. In a realistic experiment, plasma density smoothly varies between $N(z) = 0$ (vacuum region) and $N(z) = N_0$ (density plateau). Electromagnetic waves must be coupled from the vacuum side into the plasma. The effect of the plasma density inhomogeneity on the entrance of electromagnetic waves into and the exit out of the plasma must be understood. We use the fluid code to model these effects and to design the most optimal for coupling axial magnetic field profile $B_0(z)$.

## II. Derivation of Linearized Fluid Equations

We consider a one-dimensional (1-D) fluid model of the electromagnetic wave propagation in the magnetized plasma. The total magnetic field consists of the axial $B_0(z)\boldsymbol{e}_z$ and transverse (undulating) $B_u(\boldsymbol{e}_x \sin k_0 z + \boldsymbol{e}_y \cos k_0 z)$ fields. Although additional magnetic field components need to be introduced to exactly satisfy the $\boldsymbol{\nabla} \cdot \boldsymbol{B} = 0$ and $\boldsymbol{\nabla} \times \boldsymbol{B} = 0$ equations, those are dropped by neglecting the transverse variations of all field quantities. Ion motion is neglected, and plasma electrons are described as a fluid characterized by its velocity $\boldsymbol{v}$. Electron plasma is assumed cold. This assumption is justified by the high phase velocities of the resulting plasma wave. More details on the thermal effects on UIT can be found in [8]. Linearized fluid equations for the transverse and longitudinal components of the electron velocity are

$$\frac{\partial \mathbf{v}_\perp}{\partial t} + \Omega_0[\mathbf{v}_\perp \times \mathbf{e}_z] = -\frac{e}{m}\left[\mathbf{E}_\perp + \frac{v_z}{c}[\mathbf{e}_z \times \mathbf{B}_u]_\perp\right] \quad (1)$$

$$\frac{\partial v_z}{\partial t} = -\frac{e}{m}\left[E_z + \frac{1}{c}[\mathbf{v}_\perp \times \mathbf{B}_u]_z\right]. \quad (2)$$

Equations (1), (2) explicitly show that transverse and longitudinal degrees of motion are coupled by the magnetic undulator.

Linearized equation for the longitudinal and electric field component of the plasma wave simplifies in the 1-D limit to

$$\frac{\partial E_z}{\partial t} = \frac{m}{e}\omega_p^2 v_z. \quad (3)$$

The wave equation for the transverse field components is

$$\frac{\partial^2 \mathbf{E}_\perp}{\partial z^2} - \frac{1}{c^2}\frac{\partial^2 \mathbf{E}_\perp}{\partial t^2} = -\frac{m\omega_p^2}{ec^2}\frac{\partial \mathbf{v}_\perp}{\partial t}. \quad (4)$$

Because the axial magnetic field introduces the asymmetry between the RHCP and LHCP waves, it is convenient to expand the transverse components of both the electric field and electron velocity as the superposition of the right- and left-hand circularly polarized components

$$e\mathbf{E}_\perp/(mc\omega) = \mathrm{Re}[(a_+\mathbf{e}_+ + a_-\mathbf{e}_-)\exp(-i\omega t)] \quad (5)$$

$$\mathbf{v}_\perp/c = \mathrm{Re}[(\beta_+\mathbf{e}_+ + \beta_-\mathbf{e}_-)\exp(-i\omega t)]. \quad (6)$$

Here, $\mathbf{e}_+ = e_x + ie_y, \mathbf{e}_- = e_x - ie_y$. Inserting these expressions for $\mathbf{E}$ and $\mathbf{v}$ into (1), (2) and taking into account the expression for the longitudinal electric field (3), the transverse and longitudinal velocity components can be related to each other as

$$\beta_+ = \frac{\omega}{i(\omega - \Omega_0)}a_+ - \frac{\Omega_R}{\omega - \Omega_0}\beta_z \exp(ik_u z) \quad (7)$$

$$\beta_- = \frac{\omega}{i(\omega + \Omega_0)}a_- + \frac{\Omega_R}{\omega + \Omega_0}\beta_z \exp(-ik_u z) \quad (8)$$

$$\beta_z = \frac{2\Omega_R \omega}{\omega^2 - \omega_p^2}(\beta_- e^{ik_u z} - \beta_+ e^{-ik_u z}) \quad (9)$$

where $\beta_z = v_z/c$, $\Omega_R = eB_u/2mc$ is the Rabi frequency [7] proportional to the undulator strength. The Rabi frequency can be expressed as $\Omega_R = \mu_B B/\hbar$, where $\mu_B = e\hbar/2mc$ is the Bohr magneton. It is introduced by analogy with the atomic physics, where the Rabi frequency is defined as $\Omega_R = dE_0/\hbar$ (with $d$ the electric dipole moment and $E_0$ the pump electric field).

The set (7)–(9) can now be solved, and all the velocity components resolved in terms of the LHCP and RHCP electric field components

$$\beta_+ = -i\omega\frac{2\Omega_R^2\omega - \left(\omega^2 - \omega_p^2\right)(\omega + \Omega_0)}{4\Omega_R^2\omega^2 - \left(\omega^2 - \omega_p^2\right)(\omega^2 - \Omega_0^2)}a_+ - i\omega\frac{2\Omega_R^2\omega\exp(2ik_u z)}{4\Omega_R^2\omega^2 - \left(\omega^2 - \omega_p^2\right)(\omega^2 - \Omega_0^2)}a_- \quad (10)$$

$$\beta_- = -i\omega\frac{2\Omega_R^2\omega - (\omega^2-\omega_p^2)(\omega-\Omega_0)}{4\Omega_R^2\omega^2 - \left(\omega^2-\omega_p^2\right)\left(\omega^2-\Omega_0^2\right)}a_- - i\omega\frac{2\Omega_R^2\omega\exp\left(-2ik_uz\right)}{4\Omega_R^2\omega^2 - \left(\omega^2-\omega_p^2\right)\left(\omega^2-\Omega_0^2\right)}a_+. \quad (11)$$

The single-helicity theory neglected the cross-polarization effect described by (10), (11): the LHCP component of the electric field acts on the RHCP of the velocity, and the RHCP component of the electric field acts on the LHCP of the velocity. As will be shown below, the cross-polarization effect may result in a strong coupling between electromagnetic waves of opposite helicities, thereby modifying wave propagation for a broad range of undulator wavenumbers $k_u$.

Equation (10) may be simplified to make a direct connection to the single-helicity theory of UIT. Noting that UIT occurs in the vicinity of the cyclotron resonance and neglecting cross-polarization, we obtain

$$\beta_+ \approx +ia_+\frac{2\omega^2\left(\omega^2-\bar{\omega}_p^2\right)}{4\Omega_R^2\omega^2 - \left(\omega^2-\bar{\omega}_p^2\right)\left(\omega^2-\Omega_0^2\right)} \quad (12)$$

where $\bar{\omega}_p = \sqrt{\omega_p^2+\Omega_R^2}$ is the renormalized by the undulator electron plasma frequency. The standard UIT regime is obtained when $\Omega_0 = \bar{\omega}_p$, in which case (12) further simplifies to $\beta_+ = +ia_+\omega\delta\omega/(\Omega_R^2 - \delta\omega^2)$, where $\delta\omega = \omega - \Omega_0$ is the detuning from the cyclotron resonance. Because the transverse electron velocity vanishes at the resonance, no transverse currents are induced in the plasma. From (4), the electromagnetic wave with frequency $\omega = \Omega_0$ propagates as if in vacuum, i.e., its refractive index is equal to unity and the dispersion relation is $\omega^2 = k_z^2c^2$. As will be shown below, cross-polarization changes this conclusion for a significant range of undulator wavenumbers. Not only the wave may not propagate as in vacuum, it may not even be able to penetrate the plasma.

We refer to the case of $\omega^2 = k_z^2c^2$ as "perfect" transparency: plasma is transparent to the wave that would have been absorbed without the undulator. "Perfect" UIT is predicted by the single-helicity theory to take place when all relevant frequencies match: $\omega = \Omega_0 = \bar{\omega}_p$, where $\Omega_0$ and $\bar{\omega}_p$ are the cyclotron and the electron plasma frequencies in the uniform section of the plasma. In the rest of this paper, we concentrate on this frequency-matched case. Because of the natural ramp-up of the plasma density between the vacuum and the uniform plasma regions, the above frequency matching cannot be satisfied everywhere in the plasma. Moreover, it will be shown to be advantageous to use a nonuniform magnetic field to improve the coupling from the vacuum into the uniform plasma regions.

After substituting $\beta_\pm$ from (10), (11) into (4), a system of coupled equations for the $a_\pm$ amplitudes is obtained

$$\left[\frac{\partial^2}{\partial z^2} + \frac{\omega^2}{c^2}n_+^2(z)\right]a_+ = \frac{\omega^2}{c^2}g(z)e^{2ik_uz}a_- \quad (13)$$

$$\left[\frac{\partial^2}{\partial z^2} + \frac{\omega^2}{c^2}n_-^2(z)\right]a_- = \frac{\omega^2}{c^2}g(z)e^{-2ik_uz}a_+ \quad (14)$$

where the refractive indices $n_\pm$ for the RHCP and LHCP polarizations, respectively, are

$$n_\pm^2 = 1 - \frac{\omega_p^2}{\omega}\cdot\frac{2\Omega_R^2\omega - \left(\omega^2-\omega_p^2\right)\left(\omega\pm\Omega_0\right)}{4\Omega_R^2\omega^2 - \left(\omega^2-\omega_p^2\right)\left(\omega^2-\Omega_0^2\right)} \quad (15)$$

and the spatial dependencies of the refractive indices on $z$ comes from the parametric dependence of $n_\pm$ on the spatially inhomogeneous plasma density and axial magnetic field. Without an undulator, the expressions for refraction indices revert to the usual [12] formulas for the RHCP and LHCP waves propagating along the magnetic field in the plasma: $n_\pm^2 = 1-\omega_p^2/\omega(\omega\mp\Omega_0)$. Note from (15) that both $n_\pm$ are independent of $k_u$. However, it will be shown that wave propagation in the UIT plasma strongly depends on $k_u$. This is because the two polarizations are coupled.

The spatially varying coupling coefficient $g$ responsible for the cross-polarization coupling

$$g = \frac{\omega_p^2}{\omega^2}\frac{2\Omega_R^2\omega^2}{4\Omega_R^2\omega^2 - \left(\omega^2-\omega_p^2\right)\left(\omega^2-\Omega_0^2\right)} \quad (16)$$

vanishes without an undulator ($\Omega_R$) as it should because RHCP and LHCP are the eigenmodes of the uniformly magnetized plasma. Of course, the $a_\pm$ amplitudes only characterize the transverse components of the electric field of the hybrid wave. Its longitudinal electric field, $E_z = (mc\omega/e)\times \mathrm{Re}[a_z\exp -i\omega t]$, which must significantly exceed its transverse field for large energy compression to occur, is proportional to the dimensionless parameter $a_z$ given by

$$a_z = \frac{g(\omega+\Omega_0)}{\Omega_R}a_+e^{-ik_uz} - \frac{g(\omega-\Omega_0)}{\Omega_R}a_-e^{ik_uz}. \quad (17)$$

The linear fluid theory breaks down for $|a_z| \approx 1$ due to wave-breaking. Note that because under the UIT conditions $|\delta\omega| \ll \Omega_0$, the longitudinal electric field is determined primarily by the RHCP electric field component $a_+$.

## III. Analysis of Coupled-Wave Equations

The set of (13), (14) constitute the starting point of the coupled-wave theory developed below. The single-helicity theory assumes that the coupling constant $g = 0$ and neglects the excitation of the LHCP wave by the RHCP wave launched into the plasma. As shown below, this assumption cannot be justified for a wide range of $k_u$. As a result, an LHCP wave is generated according to (14) and affects the propagation of the original RHCP wave according to (13). To develop a qualitative intuition for this effect, it is helpful to approximately evaluate the refractive indices $n_\pm$ under the UIT conditions.

Since the LHCP wave does not resonantly interact with the plasma, the effect of a weak undulator is small and $n_-^2 \approx 1/2$ near the cyclotron resonance. By definition, close to perfect transparency $n_+^2 \approx 1$. The coupling constant $g$ evaluated for the perfect transparency condition is $g \approx 1/2$. Therefore, the coupling term is never small. However, in some cases, mode coupling may still be small. Note that in the absence of coupling each polarization propagates with its own wavenumber: $k_- = \pm\omega n_+/c$ and $k_- = \pm\omega n_-/c$, where $+$ and $-$ signs

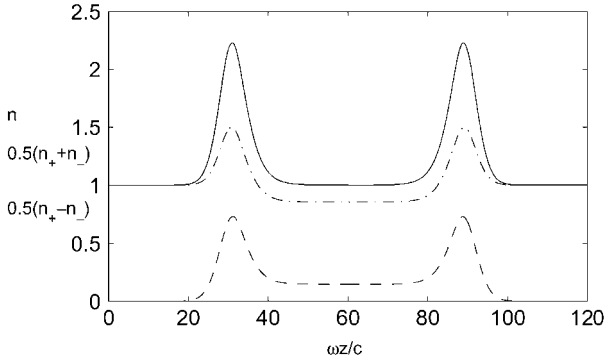


Fig. 1. Refractive indices plots for the weak undulator limit of $B_u = 0.2B_0$. Solid line: $n_+$, dash-dotted line: $[n_+(z) + n_-(z)]/2$, and dashed line: $[n_+(z) - n_-(z)]/2$ for the density and $B_0$-field profiles given by (18), (19). "Perfect transparency" regime $\omega = \Omega_0 = \bar{\omega}_p$ ensures that $n_+ = 1$ inside the plasma. Strong coupling between co-propagating and counter-propagating waves are expected for $|n_+ - n_-| = 2n_u$ and $|n_+ + n_-| = 2n_u$, respectively.

refer to forward and backward propagation directions. Therefore, in the limit of small coupling the two polarizations do not interact unless one of the two resonant conditions is satisfied: (i) $|n_+ + n_-| = 2n_u$, or (ii) $|n_+ - n_-| = 2n_u$, where $n_u = ck_u/\omega$. Case (i) corresponds to strong coupling between counter-propagating waves, and is referred to as the counter-propagating resonance. Case (ii) corresponds to strong coupling between co-propagating waves, and is referred to as the co-propagating resonance. Of course, both $n_+$ and $n_-$ are functions of $z$ for a nonuniform plasma and axial magnetic field. However, the strongest interaction is anticipated when one of the two resonances occurs in the uniform section of the plasma: waves can interact over a longer distance. To study resonant coupling between the two wave polarizations, we have assumed a specific electron density profile representing a plasma slab with smooth boundaries

$$\frac{2N(z)}{N_0} = \tanh\left(\frac{\omega z/c - 25}{5}\right) - \tanh\left(\frac{\omega z/c - 95}{5}\right) \quad (18)$$

where $40 < \omega z/2\pi c < 70$ is the density plateau. A "magnetic trap" profile of the axial magnetic is given by

$$\frac{2B(z)}{B_0} = 4 - \tanh\left(\frac{\omega z/c - 25}{5}\right) + \tanh\left(\frac{\omega z/c - 95}{5}\right). \quad (19)$$

The choice of the magnetic field profile is deliberately made to avoid the singularities of $n_\pm$. Note from (15) that the denominators are always positive if $\omega_p(z) < \omega < \Omega_0(z)$. The plots of $z$-dependent $n_+$, $n_+ + n_-$, and $n_+ - n_-$ corresponding to the density and $B_0$ field profiles given by (18), (19) are shown in Fig. 1. The choice of the "perfect" transparency parameters ensures that $n_+ = 1$ in the plateau region. From Fig. 1, observe that the co-propagating resonances are expected for $0.15 < n_u < 0.7$ (peak and plateau values of $(n_+ - n_-)/2$), while the counter-propagating resonances are expected for $0.85 < n_u < 1.5$ (peak and plateau values of $(n_+ + n_-)/2$). Of course, these small-$g$ predictions are only approximate, and direct numerical integration of (13), (14) is necessary.

### A. Numerical Simulations of the Coupled-Wave Equations

Equations (13), (14) have been numerically integrated for the most interesting case of the RHCP electromagnetic wave incident from vacuum onto the plasma layer. Perfect transparency conditions $\omega = \Omega_0 = \bar{\omega}_p$, and $B_u = 0.2B_0$ (or $\Omega_R/\omega = 0.1$) are assumed. Deviations from the perfect transparency conditions will be studied in the future publications. Boundary conditions at the left boundary of the computational domain ($z = 0$) corresponding to the RHCP wave with amplitude $a_+^{\rm inc}$ incident from the left on the vacuum-plasma boundary are imposed

$$\left[a_+ - i\frac{c}{\omega}\frac{\partial a_+}{\partial z}\right]_{z=0} = 2a_+^{\rm inc} \quad \left[a_- - i\frac{c}{\omega}\frac{\partial a_-}{\partial z}\right]_{z=0} = 0. \quad (20)$$

The choice of $a_+^{\rm inc}$ is arbitrary in the context of the linear UIT theory described by (13), (14). In fully–relativistic PIC simulations described in Section V, $a_+^{\rm inc} = 10^{-4}$ is used to ensure the linearity of the plasma response. Boundary conditions at the right boundary of the computational domain ($\omega z/c = 120$) ensures that there is no incident radiation from the right

$$\left[a_+ + i\frac{c}{\omega}\frac{\partial a_+}{\partial z}\right]_{z=L} = 0 \quad \left[a_- + i\frac{c}{\omega}\frac{\partial a_-}{\partial z}\right]_{z=L} = 0. \quad (21)$$

Depending on the undulator wavenumber $k_u$, we identified three different regimes of wave propagation and mode coupling.

*1) Small Undulator Wavenumbers, $ck_u/\omega \ll 1$:* For small undulator numbers ($0 < n_u < 0.5$), propagation regime is similar to small angle propagation with respect to constant magnetic field. Although the incident RHCP electromagnetic wave does penetrate into plasma, its propagation is very different from the "perfect" UIT described by the single-helicity theory. Electric field profiles for a characteristic example of $n_u = 0.2$ is shown in Fig. 2. Two features of the small-$n_u$ propagation are apparent from Fig. 2. First, the RHCP wave in the plateau region is not harmonic: two wavenumbers ($k_+^{(1)} = 1.32\omega/c$ and $k_+^{(2)} = 0.66\omega/c$) are present. None of these waves has phase velocity equal to $c$, as predicted by the single-helicity theory. Second, two LHCP waves are excited in the plateau region, with $k_-^{(1)} = 0.92\omega/2$ and $k_-^{(2)}c = 0.26\omega/c$. No reflection from the plasma slab was found, but almost 16% of the incident RHCP energy was converted into the LHCP wave after transiting the plasma. Because the amplitude of the LHCP and RHCP are comparable in the plasma, we conclude that the RHCP undergoes an efficient conversion into LHCP upon entering the plasma. This is undesirable from the accelerator applications standpoint because the amplitude of the accelerating field $a_z$ is determined only by $a_+$. The longitudinal plasma wave in the plateau region also contains two spatial harmonics: $k = 1.12\omega/c$ and $k = 0.46\omega/c$.

The substantial difference in the wave propagation for small $n_u$ from the predictions of the single-helicity theory can be attributed to the strong interaction between *co-propagating* RHCP and LHCP. Although plasma is transparent in this regime, the details of the wave propagation are significantly altered, and substantial mode conversion is observed. As shown

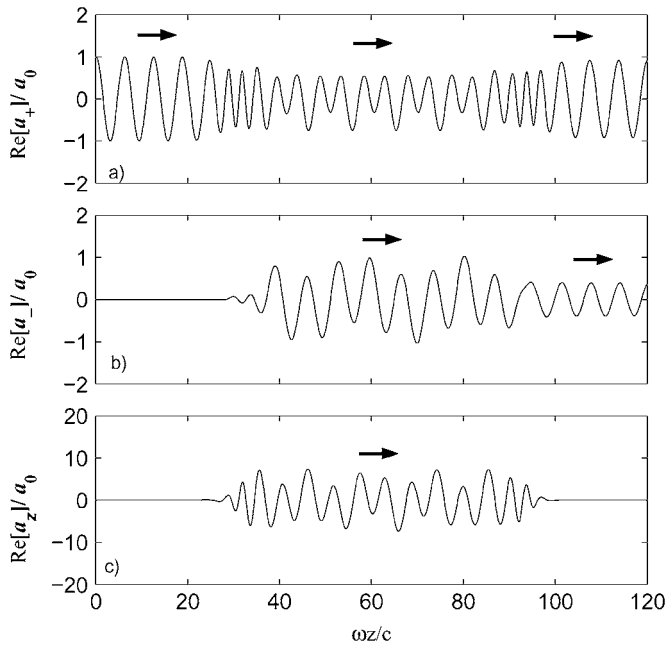


Fig. 2. Amplitudes of the electromagnetic wave components in the UIT plasma normalized to that of the injected RHP wave $a_+^{\rm inc} = a_0$: (a) the transverse RHP, (b) the transverse LHP, and (c) the longitudinal components of the electric field in the "small angle propagation" regime ($n_u = 0.2$), undulator strength $B_u = 0.2B_0$, $\omega = \Omega_0$, $\bar{\omega}_p = \Omega_0$. Arrows indicate the direction of the phase velocity.

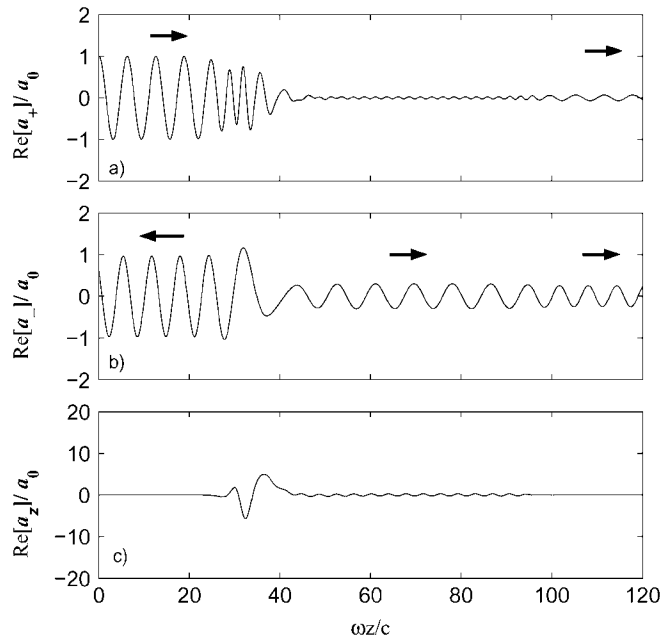


Fig. 3. Same as Fig. 2, but $n_u = 0.9$. Plasma is opaque to the RHCP wave.

below, larger undulator wavenumbers can couple *counter-propagating* RHCP and LHCP waves, making plasma completely opaque to the forward-propagating RHCP.

*2) Moderate Undulator Wavenumbers, $ck_u/\omega \sim 1$:* For ($n_u \sim 1$), wave propagation is even more different from the "perfect" UIT predicted by the single-helicity theory. This is illustrated by Fig. 3(a) which shows that the plasma is opaque to RHCP wave which does not penetrate into the plateau region. The opaqueness is caused by the strong counter-propagating

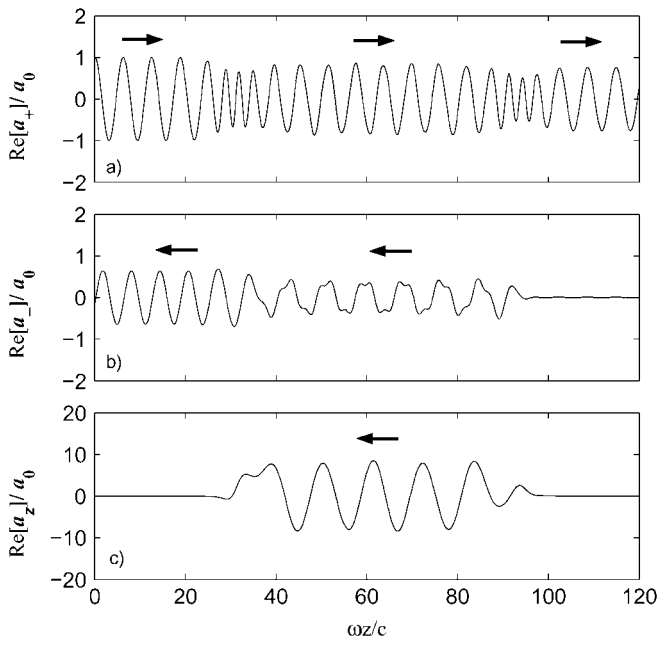


Fig. 4. Same as Fig. 2, but $n_u = 1.6$. Both plasma transparency and energy compression are observed.

resonance: the forward-travelling RHCP mode-converts into the backward-travelling LHCP. This is evident from Fig. 3(a): almost the entire energy of the RHCP incident wave is reflected with the change in the polarization (about 90%). The remaining 10% is mode-converted into the forward-traveling LHCP which penetrates into the plateau region of the plasma and subsequently leaves the plasma from the right side. The plasma wave has a very small amplitude compared to the previous $n_u = 0.2$ because of the small RHCP component of the electric field in plasma plateau region.

*3) Large Undulator Wavenumbers, $ck_u/\omega \gg 1$:* Increasing the undulator wavenumber results in the wave propagation which is in a good agreement with the single-helicity theory, i.e., "perfect" UIT. Transverse and longitudinal field profiles corresponding to $n_u = 1.6$ are shown in Fig. 4. About 60% of the incident RHCP energy propagates across the plasma slab (amplitude transmission coefficient for RHP is $T_+ = E_+/E_{\rm inc} \approx 0.76$), with the remaining 40% mode-converted into the LHCP wave (amplitude reflection coefficient $R_- = E_-/E_{\rm inc} \approx 0.64$) and reflected out of the plasma.

From Fig. 4(a) and (b), we observe that the RHCP wave dominates in the plasma plateau region, resulting in a strong harmonic plasma wave, shown in Fig. 4(c). Note that the peak plasma wave amplitude is ten times higher than that of the incident RHCP wave: $Q = E_z^{(\max)}/E_{\rm inc}^{(\max)} \approx 10$. This enhancement is the manifestation of the energy density compression by a factor $G = Q^2/2 \approx 50$, in good agreement with the single-helicity calculation of the group velocity $v_g/c = 2\Omega_R^2/\Omega_0^2 = 50$. Note that the phase velocity of the plasma wave is opposite to the phase and group velocities of the RHCP wave in the plasma. One can thus envision novel types of plasma-based backward-wave oscillators (BWO), in which electron beams propagating in $-z$ direction resonantly interact with slow electromagnetic waves propagating in $+z$ direction.

The wavenumber of the RHCP wave in the plasma is $k_+ = \omega/c$ in agreement with the single-helicity theory. For larger undulator wavenumbers, the reflection further decreases, and the transparency become perfect. Thus, we conclude that the single-helicity UIT theory which was originally used to predict the "perfect" UIT is only valid for large $n_u > 1.6$.

## IV. WKB Approach to Solving the Coupled-Wave Equations

Analytic insight into the numerical solutions presented in Section III can be gained by assuming that all plasma and magnetic field parameters are adiabatically slowly varying on the wavelength scale $\sim c/\omega$. Under the adiabatic assumption, geometric optics can be used, and electromagnetic waves in the plasma can be described using phase-space trajectories in the $(n, z)$ phase plane [13]. The resulting approximate description of the wave propagation is equivalent to the multicomponent Wentzel–Kramers–Brillouin (WKB) theory developed in [14], [15]. The WKB description assigns propagation trajectories in the $(n, z)$ phase plane to different electromagnetic modes. One aspect of wave propagation that is not captured by WKB is tunneling between different phase-space trajectories. Although powerful techniques have been developed to estimate tunnelling probabilities [16]–[18], those are beyond the scope of the present work. Our emphasis is on the utility of geometric optics for *qualitative* prediction of the effects of mode coupling on the wave propagation.

To apply WKB to the governing system of (13), (14), it is convenient to apply the following linear transformation which eliminates the rapidly oscillating in $z$ coefficients in the right-hand sides

$$a_\pm = \tilde{a}_\pm \exp(\pm \mathrm{i} n_u \tilde{z}) \tag{22}$$

where the normalized spatial variable $\tilde{z} = \omega z/c$ is introduced. From (13), (14) we obtain

$$\frac{\partial^2 \tilde{a}_+}{\partial \tilde{z}^2} + 2\mathrm{i} n_u \frac{\partial \tilde{a}_+}{\partial \tilde{z}} + \left(n_+^2 - n_u^2\right) \tilde{a}_+ = g \tilde{a}_- \tag{23}$$

$$\frac{\partial^2 \tilde{a}_-}{\partial \tilde{z}^2} - 2\mathrm{i} n_u \frac{\partial \tilde{a}_-}{\partial \tilde{z}} + \left(n_-^2 - n_u^2\right) \tilde{a}_- = g \tilde{a}_+ \tag{24}$$

where $n_\pm$ are slowly varying with $\tilde{z}$.

The two-component WKB solutions corresponding to various propagation branches (labeled by the index $\mu$) can be found in the following form:

$$\mathbf{A}^{(\mu)}(\tilde{z}) = B^{(\mu)}(\tilde{z}) \mathbf{U}^{(\mu)}(\tilde{z}, n) \exp\left( i \int^{\tilde{z}} n^{(\mu)}(\tilde{z})\, d\tilde{z} \right) \tag{25}$$

where $\mathbf{A}^{(\mu)}(z) = [\tilde{a}_+^{(\mu)}\ \tilde{a}_-^{(\mu)}]^T$, $\mathbf{U}^{(\mu)}$, and $B^{(\mu)}(\tilde{z})$ are the unit vector and amplitude of the $\mu$th propagation branch, respectively. The unit vector $\mathbf{U}^{(\mu)}$ is found from the dispersion matrix $D(\tilde{z}, n)$ which is obtained by introducing a local wavenumber $-id/d\tilde{z} \equiv n(\tilde{z})$:

$$D(\tilde{z}, n) = \begin{pmatrix} D_+(\tilde{z}, n) & g(\tilde{z}) \\ g(\tilde{z}) & D_-(\tilde{z}, n) \end{pmatrix} \tag{26}$$

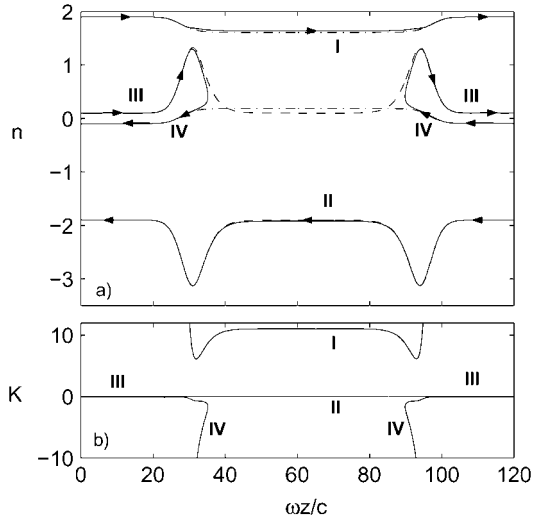


Fig. 5. Geometric optics approach to wave propagation of two coupled polarizations, $n_u = 0.9$. (a) Solid lines: phase space trajectories calculated from (28). Arrows indicate group velocity direction. Dashed line and dot-dashed lines: noninteracting ($g = 0$) forward RHCP and backward LHCP. (b) Mode ratios $K$ from (29) for various propagation branches. Only branches I (forward LHCP) and II (backward RHCP) propagate through the entire plasma slab. Small $K \ll 1$ corresponds to the predominantly RHCP mode. Magnetic field and plasma parameters: same as in Fig. 3.

where $D_\pm(z, n) = (n \pm n_u)^2 - n_\pm^2(\tilde{z})$. The orthonormal eigenvectors $\mathbf{U}^{(\mu)}$ are obtained by solving the following equation:

$$D_{\alpha\beta}(\tilde{z}, n) U_\beta^{(\mu)}(\tilde{z}, n) = 0 \tag{27}$$

where index $\mu$ labels different propagation branches. It is shown below that depending on $z$, there could be two or four different propagation branches. For example, in the plasma regions where both forward and backward waves of both polarizations (RHCP and LHCP) exist, there are four propagation branches.

Equation (27) can have nontrivial solutions only if the determinant of the dispersion matrix $D_{\alpha\beta}$ is zero

$$[(n + n_u)^2 - n_+^2(\tilde{z})][(n - n_u)^2 - n_-^2(\tilde{z})] = g^2(\tilde{z}). \tag{28}$$

By calculating $n^{(\mu)}(\tilde{z})$ that satisfy (28), a phase space trajectory in the $(n, \tilde{z})$ phase space can be drawn. A typical example for $n_u = 0.9$ is shown in Fig. 5(a). Note that the local wavenumber $k \equiv n\omega/c$ has a clear physical meaning: it is equal to the wavenumber of the longitudinal plasma wave. The wavenumbers of the RHCP (LHCP) are obtained from $k$ by simply adding (subtracting) the undulator wavenumber $k_u$. A useful quantity characterizing any given propagation branch is the mode amplitude ratio (LHP over RHP) $K(z, n) \equiv U_2^{(\mu)}/U_1^{(\mu)}$ which can be calculated from (27)

$$K(z, n) = -\frac{(n + n_u)^2 - n_+^2(z)}{g(z)} \tag{29}$$

where $K \ll 1$ corresponds to the dominance of the RHCP mode. Mode ratio for two propagation branches labeled as I and II are plotted in Fig. 5(b).

We are now in a position of relating the phase space trajectories shown in Fig. 5 to the full numerical simulations results presented in Fig. 3. According to Fig. 5(a), four propagating branches exist at the entrance into the plasma ($z < 35c/\omega_p$).

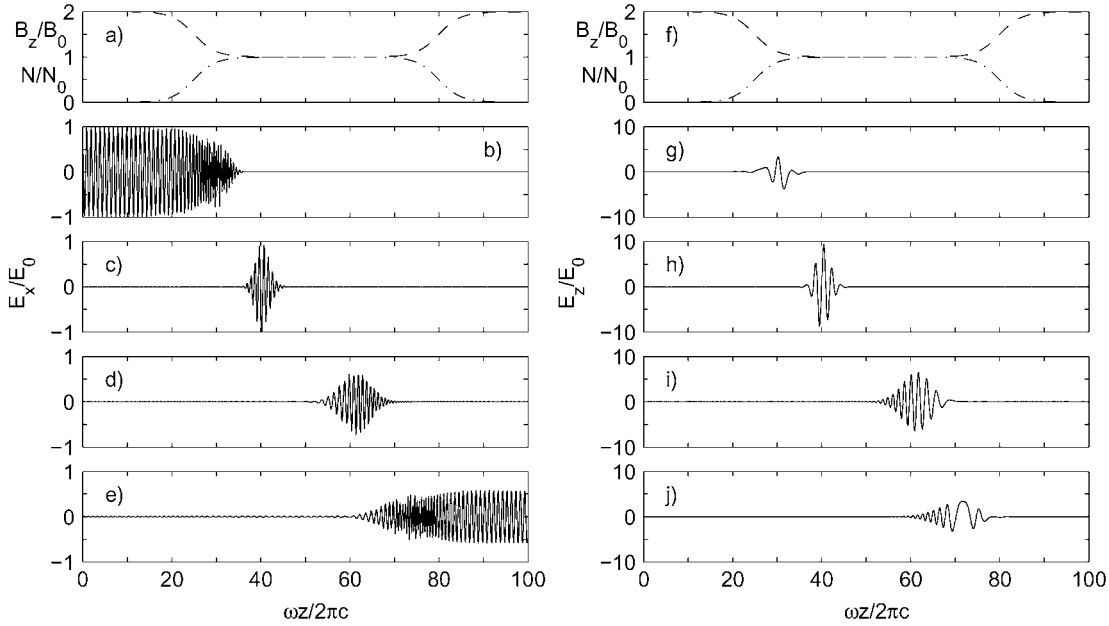


Fig. 6. Sequential snapshots at $t = t_i$ of the time evolution of the transverse [left column, (b)–(e)] and longitudinal [right column, (h)–(j)] electric field normalized to the electric field in the incident wave, $a_+^{\rm inc} = 10^{-4}$. (b) and (g): $t_1 = 211.2\lambda/c$; (c) and (h): $t_2 = 614.4\lambda/c$; (d) and (i): $t_3 = 1632\lambda/c$; (e) and (j): $t_4 = 2285\lambda/c$. Top figures [(a) and (f)] are the normalized electron density and axial magnetic field spatial profiles. Parameters: same as in Fig. 3.

However, only two branches exist inside the plasma. This implies that the RHCP launched at $z = 0$ does not penetrate into the plasma. Instead, it undergoes a complete mode transformation into the LHCP wave and is reflected out of the plasma. This is essentially what is observed in Fig. 3(a). For comparison, the unperturbed by the cross-polarization interaction $(g = 0)$ phase space trajectories are also indicated in Fig. 3(a) by the dashed (forward RHCP) and dot-dashed (backward LHCP) lines. The close proximity of the unperturbed phase space trajectories indicates that the condition for the counter-propagating resonance is almost fulfilled. This is why the ray trajectories are strongly perturbed by the cross-polarization interaction.

The detailed comparison between Figs. 3 and 5 also reveals the limitations of the geometric optics approach. For example, Fig. 3(b) indicates that a small-amplitude LHCP wave does penetrate into the plasma. Qualitatively, this is caused by the finite tunnelling of the launched wave III (in the middle of the phase space) into the forward-propagating wave I that is predominantly LHCP. The WKB theory by itself does not account for such tunnelling, and needs to be extended if the tunnelling coefficient is desired. Rigorous calculation of the tunnelling coefficients is beyond the scope of this work, and will be addressed in the future publications.

## V. Particle-in-Cell Simulations of Energy Compression

In order to confirm the results of the linearized single-frequency fluid calculation of UIT in a cold magnetized plasma, and to study the time-dependent properties of UIT, we used the 1-D version of the fully electromagnetic PIC code VLPL [19]. The following simulation parameters have been used: grid size $\delta z = 0.1\lambda$ (where $\lambda = 2\pi c/\omega$ is the vacuum wavelength of the incident radiation), 128 particles per cell. The case of $n_u = 1.6$, which most closely approached the "perfect" UIT regime, has been simulated with $\omega = \Omega_0 = \bar{\omega}_p$, and the helical undulator strength $B_u = 0.2B_0$ was chosen. Here, $B_0$ is the axial magnetic field in the plasma plateau region. These are the same undulator, density, and axial magnetic field parameters that were used in the linearized fluid single-frequency simulations described in Fig. 3. PIC simulations were performed in the time domain, and a finite-duration Gaussian pulse with the duration $T = 100\lambda/c$ and the peak amplitude $a_+^{\rm inc} = 10^{-4}$ was injected into the magnetized plasma. The incident pulse was right-hand circularly polarized.

Electron plasma was assumed to be initially quiescent. Electron plasma density profile is chosen to have a smooth vacuum/plasma interface and a constant-density plateau region $20 < z/\lambda < 80$

$$\frac{N(z)}{N_0} = 0.5\tanh\left(\frac{z/\lambda - 20}{5}\right) - 0.5\tanh\left(\frac{z/\lambda - 80}{5}\right).$$

The axial magnetic field has the "magnetic trap" shape: gradually decreasing from a higher amplitude $(eB_z/mc = 2\omega)$ in the low-plasma density regions to the "perfect" UIT value of $eB_0/mc \equiv \Omega_0 = \omega$ in the plasma plateau region. The exact magnetic field profile is

$$\frac{B_z}{B_0} = 2 - 0.5\tanh\left(\frac{z/\lambda - 20}{5}\right) + 0.5\tanh\left(\frac{z/\lambda - 80}{5}\right).$$

A time sequence of snapshots $t_i$ (defined in the caption to Fig. 6) of the transverse and longitudinal electric fields are shown in the left and right panels of Fig. 6, respectively. The long incident pulse is indeed shown to compress in the plasma [see Fig. 6(c)]; the fact that could be only indirectly inferred from the fixed frequency simulations. At $t = t_2$, the entire pulse is inside the plasma plateau. It is propagating with the reduced group velocity through the plasma between $t = t_2$ and $t = t_3$, advancing by $\Delta z = 20\lambda$. Hence, the group velocity $v_{\rm gr} = \Delta z/(t_3 - t_2) \approx 0.02c$ is in excellent agreement with the theoretical estimate of $v_{\rm gr} = cB_u^2/2B_0^2$.

While the pulse is inside the plasma, the amplitude of the longitudinal electric field is almost 10-fold of the incident RHCP wave, as shown in Fig. 6(h). The large value of the longitudinal electric field makes UIT plasma an attractive candidate for electron and ion acceleration. Phase velocity of the accelerating field can be controlled by tapering the undulator period as a function of $z$.

Radiation exits the plasma at $t = t_4$. Close inspection of the longitudinal field at $t = t_4$ indicates that the exiting pulse is strongly chirped: short wavelengths are propagating faster than the long wavelengths. This effect is very pronounced despite the very long pulse duration $T$ because of the strongly dispersive nature of the UIT plasma [9]. This group velocity dispersion effect can only be revealed by time-dependent simulations. Note that the outdoing chirped pulse is broadened by the interaction. This happens because, in the linear regime, the total pulse bandwidth remains the same. Therefore, the chirped pulse must be longer than the bandwidth limited input pulse.

## VI. Conclusion

In conclusion, we have demonstrated using PIC simulations that extreme energy compression of electromagnetic radiation is possible in a magnetized plasma made transparent by an addition of a weak helical undulator. For this compression to occur, a right-hand circularly polarized electromagnetic wave has to be coupled into the plasma at the electron cyclotron frequency. Although without an undulator this wave would be absorbed by the plasma via electron cyclotron heating, plasma becomes transparent due to the phenomenon of UIT. Because the electromagnetic wave in the UIT plasma is primarily longitudinal, it can be useful for various accelerator applications.

Realistic plasma density and magnetic field profiles were accounted for, and the efficiency of radiation coupling into the plasma studied. It was found that the extreme energy compression occurs only for large undulator wavenumbers. For some wavenumbers, plasma remains opaque. This strong dependence of the propagation properties through the UIT plasma was found to be caused by cross-polarization coupling between left and right-hand circularly polarized waves. A fixed-frequency linearized fluid code was used to model cross-polarization coupling. Qualitatively, the mode coupling can be understood in the framework of geometric optics. Future work will study the large-field effects in the plasma, and investigate how an effective accelerator with the longitudinal electric field approaching wavebreaking limit can be designed.

## Acknowledgment

The authors wish acknowledge useful discussions with R. G. Littlejohn and A. N. Kaufman.

## References

[1] K. J. Boller, A. Imamoglu, and S. Harris, "Observation of electromagnetically induced transparency," *Phys. Rev. Lett.*, vol. 66, p. 2593, 1991.
[2] S. E. Harris, "Electromagnetically induced transparency," *Phys. Today*, vol. 7, p. 39, 1997.
[3] A. V. Turukhin, V. S. Sudarshanam, M. S. Shahriar, J. A. Musser, B. S. Ham, and P. R. Hemmer, "Observation of ultraslow and stored light pulses in a solid," *Phys. Rev. Lett.*, vol. 88, p. 023 602, 2002.
[4] S. Chesi, M. Artoni, G. C. L. Rocca, F. Bassani, and A. Mysyrowicz, "Polaritonic stop-band transparency via exciton-biexciton coupling in cucl," *Phys. Rev. Lett.*, vol. 91, p. 057 402, 2003.
[5] A. B. Matsko, Y. V. Rostovtsev, M. Fleischhauer, and M. O. Scully, "Anomalous stimulated brillouin scattering via ultraslow light," *Phys. Rev. Lett.*, vol. 86, p. 2006, 2001.
[6] A. G. Litvak and M. D. Tokman, "Electromagnetically induced transparency in essembles of classical oscillators," *Phys. Rev. Lett.*, vol. 88, p. 095 003, 2002.
[7] G. Shvets and J. S. Wurtele, "Transparency of magnetized plasma at the cyclotron frequency," *Phys. Rev. Lett.*, vol. 89, p. 115 003, 2002.
[8] A. Y. Kryachko, A. G. Litvak, and M. D. Tokman, "The effect of electromagnetically induced transparency in magnetoactive high temperature plasmas," *Nuc. Fus.*, vol. 44, p. 414, 2004.
[9] G. Shvets and M. Tushentsov, "Nonlinear propagation of electromagnetic waves in a plasma by means of electromagnetically induced transparency," *J. Modern Optics*, vol. 50, p. 2583, 2003.
[10] M. Fleischhauer and M. D. Lukin, "Dark-state polaritons in electromagnetically induced transparency," *Phys. Rev. Lett.*, vol. 84, p. 5094, 2000.
[11] M. Hur, J. Wurtele, and G. Shvets, "Simulation of electromagnetically and magnetically induced transparency in essembles in magnetized plasma," *Phys. Plasmas*, vol. 10, p. 3004, 2003.
[12] V. Ginzburg, *The Propagation of Electromangetic Waves in Plasmas*. Oxford, U.K.: Pergamon, 1970.
[13] A. N. Kaufman and L. Friedland, "Phase-space solution of the linear mode-conversion problem," *Phys. Lett. A*, vol. 123, p. 387, 1987.
[14] R. Cairns and C. Lashmore-Davies, "A unified theory of a class of mode conversion problems," *Phys. Fluids*, vol. 26, p. 1268, 1983.
[15] A. N. Kaufman, H. Ye, and Y. Hui, "Variational formulation of covariant eikonal theory for vector waves," *Phys. Lett. A*, vol. 120, p. 327, 1987.
[16] L. Friedland and A. N. Kaufman, "Congruent reduction in geometric optics and mode conversion," *Phys. Fluids*, vol. 30, p. 3050, 1987.
[17] R. G. Littlejohn and W. G. Flynn, "Geometric phases in the asymptotic theory of coupled wave equation," *Phys. Rev. A*, vol. 44, p. 5239, 1991.
[18] ——, "General linear mode conversion coefficient in one dimension," *Phys. Rev. Lett.*, vol. 70, p. 1799, 1993.
[19] A. M. Pukhov, "Three-dimensional electromagnetic relativistic particle-in-cell code vlpl (virtual laser plasma lab.)," *APS Bull.*, vol. 41, p. 1502, 1996.

**Mikhail Tushentsov** was born in Nizhny Novgorod, U.S.S.R. (now Russia), on June 24, 1977. He received the B.S. degree in physics and the M.S. degree from the Nizhny Novgorod State University, Nizhny Novgorod, Russia, in 1998 and 2000, respectively. From 2002 to 2003, he was a graduate student at Illinois Institute of Technology, Chicago. He is currently working toward the Ph.D. degree in physics at the University of Texas, Austin.

From 1997 to 2001, he was with the Institute of Applied Physics, Russian Academy of Sciences, Nizhny Novgorod, as a Junior Research Scientist. From 1999 to 2002, he was a Guest Researcher at Chalmers University of Technology, Gothenburg, Sweden. His research has concentrated on the area of the interaction of the electromagnetic radiation with matter and advanced accelerators. He has published about ten papers and conference proceedings in refereed scientific journals.

Mr. Tushentsov has been a Student Member of the American Physical Society since 2003.

**Gennady Shvets** (M'03) was born in Kiev, U.S.S.R. (now Ukraine), in 1969. He received the Ph.D. degree in physics from the Massachusetts Institute of Technology, Cambridge, in 1995.

He is an Assistant Professor of Physics at the University of Texas, Austin. Previously he has held research positions at the Princeton Plasma Physics Laboratory, Princeton, NJ, and the Fermi National Accelerator Laboratory, Batavia, IL, and was on the faculty of the Illinois Institute of Technology, Chicago. His research interests include plasma physics, advanced particle accelerators, photonics, and nonlinear optics.

Dr. Shvets was a Department of Energy Postdoctoral Fellow, during 1995–1996. He was a recipient of the Presidential Early Career Award for Scientists and Engineers in 2000.

**Andrey Yu. Kryachko** was born in Sevastopol, U.S.S.R. (now Ukraine), in 1978. He received the M.S. degree in physics from the Nizhny Novgorod State University, Nizhny Novgorod, Russia, in 2001. He is currently working toward the Ph.D. degree at the Institute of Applied Physics, Russian Academy of Sciences, Nizhny Novgorod.

His current scientific research is mainly focused on nonlinear parametric interaction of the waves in plasma.

**Mikhail D. Tokman** was born in Nizhny Novgorod, U.S.S.R. (now Russia), in 1956. He received the M.S. degree in radiophysics and electronics from Nizhny Novgorod State University in 1979 and the Ph.D. and Dr.Sci. degrees from the Institute of Applied Physics, Russian Academy of Sciences, Nizhny Novgorod, in 1987 and 1996 respectively.

Since 1996, he has been the Principal Researcher of the Institute of Applied Physics, Nizhny Novgorod. His current research interests include the theory of resonant interaction of electromagnetic waves with ensembles of electrons in plasmas. He is the expert of the Russian Foundation for Basic Research. He has more than 100 publications in journals and conference reports.